Available online at http://scik.org
J. Math. Comput. Sci. 11 (2021), No. 1, 477-493
https://doi.org/10.28919/jmcs/5157
ISSN: 1927-5307

ELECTRO-THERMO-CONVECTION FLOW OF CONDUCTING NON-NEWTONIAN FLUID OVER UPRIGHT WAVY CONE ALONGSIDE IRREGULAR ELECTRICAL CONDUCTIVITY

HAMED M. SAYED[1,2,*], EMAD H. ALY[1,3]

[1]Department of Mathematics, Faculty of Education, Ain Shams University, Roxy 11757, Cairo, Egypt

[2]Department of Mathematics, Faculty of Science, Taibah University, Yanbu 41911, Saudi Arabia

[3]Department of Mathematics, Faculty of Science, University of Jeddah, Jeddah 21589, Saudi Arabia

Abstract. This work aims to investigate the numerical analysis of the electrohydrodynamic (EHD) effect using a Casson fluid model. The EHD flow for the laminar forced convection and heat transfer on a vertical wavy cone with variable electric conductivity in the existence of internal heat generation/absorption and Ohmic dissipation was simulated. The problem model was characterized by highly partial differential equations that were concluded via the approximation of the boundary layer. The governing model was then turned into ordinary paired differential equations that applied convenient similarity transformations. Thus, the resulted equations were numerically investigated using the Keller-box method. The impact of the different physical parameters on the velocity profiles and temperature distributions, and also on the shear stress and heat transfer rate, were presented. It was found that a decrease in the electric field parameter leads to heighten the velocity, local skin friction coefficient, and local rate of heat transfer whereas the temperature reduces. Further, rising the Eckert number was deduced to decrease the local rate of heat transfer whilst the velocity, temperature, and local skin friction coefficient were enhanced.

Keywords: forced convection; EHD; Casson fluid; electrical conductivity; Ohmic dissipation.

2010 AMS Subject Classification: 76R05, 35Q35, 76A05, 76N20, 20B40.

*Corresponding author

E-mail addresses: hmse2112@hotmail.com, hamedali@edu.asu.edu.eg

Received November 1, 2020

1. INTRODUCTION

In many engineering and manufacturing applications, roughened surfaces are commonly present. It is oftentimes developed to enhance heat transfer in heat transfer devices. The natural laminar convection flow over rough surfaces can be utilized for heat transfer in countless thermal transfer devices, for instance, flat plate condensers in refrigerators, heat exchanger, flat plate solar collectors, industrial heat radiators, geothermal reservoirs, and functional clothing design, etc. It is therefore that the investigation of the flow over the rough surface has interested many researchers in different physical situations [1-10].

It is well known that Electrohydrodynamics (EHD) is a cross-disciplinary field with important applications in industrial processes addressing the interaction among fluids, electric charges, and electrical fields [11, 12]. The effects of an electromagnetic fields on convective heat transfer are of great interest since they induce currents in the fluid. the hydrodynamic and Maxwell's equations of electromagnetism are the equations that describe this category of flow which is of considerable prominence in the industrial, technological, and geothermal applications. Further research on this type of electromagnetic fluid flow numerically can be followed through the references [13] to [20]. Many engineering applications are available for the magnetic field, which affect the heat generation/absorption processes in the conduction of electrical fluid flows [21-29].

Casson fluid is a type of visco-plastic fluids that reveals yield stress and whose constitutive equation was described by Casson [30]. Insomuch as the shear stress is weaker than the yield stress, Casson 's liquid functions like a solid and behaves like a fluid when the shear stress is larger than the yield stress. It has considerable usages in polymer treatment industries and biomechanics. Casson fluid model examples jelly, juices, honey, tomato sauce, silicon suspension, human blood, polymeric liquids, and many others. Some relevant studies about this fluid model can be seen in references [31] up to recently [36].

To the authors' knowledge, the heat transfer problems of viscous flows alongside roughened surfaces have been extensively discussed by many authors. However, solutions are not yet presented for the Casson fluid flow in the existence of an electric field together with variable electric conductivity. Therefore, The goal of the current seeking is to investigate the problem

of effects of electromagnetic field on forced convective heat transfer over a vertical wavy cone retained at an unvarying surface temperature flooded with a Casson fluid beside an irregular electric conductivity and take into consideration the internal heat generation/absorption and Ohmic heating (Joule electromagnetic dissipation) to explore the impact of the germane parameters, such as amplitude wavelength ratio, Casson fluid parameter, electrical field parameter, magnetic field parameter, Prandtl number, Eckert number and heat generation/absorption parameter on fluid velocity, temperature, local coefficient of skin friction, and local heat transfer rate. The governing nonlinear equations are constricted to ordinary differential equations via the fitting similarity transformations and then they are numerically solved applying the Keller-box implicit finite difference method.

2. FLOW ANALYSIS

The physical problem deals with the steady-state of an incompressible electrically conducive Casson fluid boundary layer flow near a wave cone whose transverse vertical sinusoidal surface. The wavy surface cone is illustrated by

$$\overline{y} = \overline{\delta}(\overline{x}) = \overline{a}\ \sin\left(\frac{\pi\overline{x}}{L}\right), \tag{1}$$

where $\overline{a}$ is the wavy surface amplitude and $2L$ is the characteristic length associated with the uneven surface. The coordinate system is defined in such a way that x-axis runs from the apex to the cone's flat surface, and y-axis is perpendicularly measured outward as seen in Fig. 1. The surface of the wave cone is assumed to be at a uniform temperature T_w and the regular ambient temperature T_∞, where $T_w > T_\infty$. Also, the region of flow is incurred to a regular electrical field $\mathbf{E} = (0,0,E_0)$ and regular transverse magnetic field $B = (0,B_0,0)$. From Maxwell's equations, it is well known that $\bigtriangledown \times E = 0$ and $\bigtriangledown \cdot \mathbf{B} = 0$. The electric field and magnetical field conform with the law of Ohm $J = \sigma(\mathbf{E} + V \times \mathbf{B})$, when the magnetic field is not vigorous, in which J is the Joule current, σ is the magnetic permeability and V is the velocity of the fluid. Therefore, the inducing magnetic field is neglected because of the motion of the electrically conductive fluid. Further, the fluid's electrical conductivity differs linearly with the component transverse velocity [37]. Consequently, the thermal energy equation contains the thermal dispersion, heat source/sink, and Joule heating owing to the magnetic in addition to electric fields. Moreover,

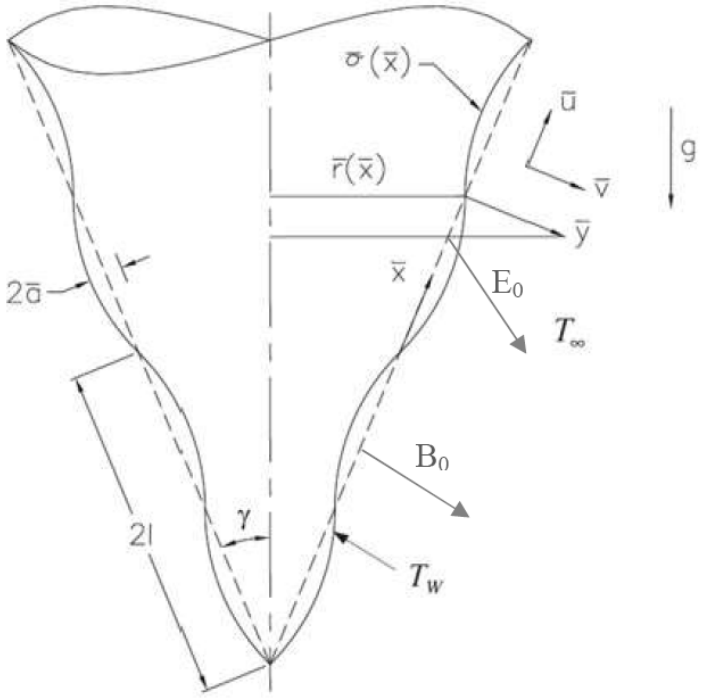

FIGURE 1. Physical model configuration and coordinate scheme.

the thermal physical characteristics should be constant except that the fluid density in the momentum equation depends on the temperature during the buoyancy force term. The dimensional equations of the problem are now built based on previous assumptions as following (see [8])

$$\frac{\partial(\bar{r}\,\bar{u})}{\partial\bar{x}}+\frac{\partial(\bar{r}\,\bar{v})}{\partial\bar{y}}=0, \tag{2}$$

$$\rho\left(\bar{u}\frac{\partial\bar{u}}{\partial\bar{x}}+\bar{v}\frac{\partial\bar{u}}{\partial\bar{y}}\right)=-\frac{\partial\bar{p}}{\partial\bar{x}}+\mu\left(1+\frac{1}{\alpha}\right)\bigtriangledown^2\bar{u}+\rho\beta g\left(\overline{T}-\overline{T}_\infty\right)\cos\gamma-\sigma B_0\left(E_0+B_0\,\bar{u}\right), \tag{3}$$

$$\rho\left(\bar{u}\,\frac{\partial\bar{v}}{\partial\bar{x}}+\bar{v}\,\frac{\partial\bar{v}}{\partial\bar{y}}\right)=-\frac{\partial\bar{p}}{\partial\bar{y}}+\mu\left(1+\frac{1}{\alpha}\right)\bigtriangledown^2\bar{v}+\rho\beta g\left(\overline{T}-\overline{T}_\infty\right)\sin\gamma, \tag{4}$$

$$\rho C_p\left(\bar{u}\,\frac{\partial\overline{T}}{\partial\bar{x}}+\bar{v}\,\frac{\partial\overline{T}}{\partial\bar{y}}\right)=k\bigtriangledown^2\overline{T}+Q_0\left(\overline{T}-\overline{T}_\infty\right)+\sigma\left(E_0+B_0\bar{u}\right)^2, \tag{5}$$

where ρ is the fluid density, ($\bar{u}$, $\bar{v}$) are the components of the velocity in ($\bar{x}$, $\bar{y}$) respectively, $\bar{r}(\bar{x})$ $(=\bar{x}\sin\gamma)$ is the local radius of the cone's flat surface, γ is the half-angle of the cone's flat surface, $\bar{p}$ is the pressure of fluid, μ is the viscosity of dynamic, α is the parameter of Casson fluid, $\bigtriangledown^2$ is the Laplacian operator, β is the volumetric expansion coefficient, g is the gravitational acceleration, $\overline{T}$ is the temperature, C_p is the specific heat at invariable pressure,

k is the fluid thermal conductivity and Q_0 is the dimensional heat generation $(Q_0 > 0)$ or heat absorption $(Q_0 < 0)$. Here σ is presumed to rely on the fluid velocity and to have the format $\sigma = \sigma_0 \overline{u}$.

The suitable boundary conditions can often be modeled as

$$\begin{aligned} \overline{u} &= 0, \qquad \overline{v} = 0, \qquad \overline{T} = \overline{T}_w \quad \text{at} \quad \overline{y} = \overline{\delta}(\overline{x}), \\ \overline{u} &= 0, \qquad \overline{T} = \overline{T}_w, \qquad \overline{p} = \overline{p}_\infty \quad \text{at} \quad \overline{y} \longrightarrow \infty. \end{aligned} \tag{6}$$

In order to dimensionless the system, we introduce the following transformations [34]

$$\begin{aligned} u &= \frac{\rho L}{\mu} Gr^{-1/2} \overline{u},\ v = \frac{\rho L}{\mu} Gr^{-1/4} \left(\overline{v} - \overline{\delta}_{\overline{x}} \overline{u} \right),\ x = \frac{\overline{x}}{L},\ r = \frac{\overline{r}}{L},\ y = \frac{\overline{y} - \overline{\delta}(\overline{x})}{L}, \\ \delta(x) &= \frac{\overline{\delta}(\overline{x})}{L},\ \frac{d\delta}{dx} = \overline{\delta}_{\overline{x}} = \frac{d\overline{\delta}}{d\overline{x}}, \quad p = \frac{L^2}{\rho \upsilon^2 Gr} \overline{p}, \quad \theta = \frac{\overline{T} - \overline{T}_\infty}{\overline{T}_w - \overline{T}_\infty}, \\ Gr &= \frac{g\beta \left(\overline{T} - \overline{T}_\infty \right) L^3 \cos\gamma}{\nu^2}, \end{aligned} \tag{7}$$

where a, Gr are the amplitude wavelength ratio and Grashof number in term of the temperature, respectively. Now, on substituting the transformations (7) into Eqs. (2) to (5) and assuming that $Gr \longrightarrow \infty$ [3], the equations system can be converted as follows in equations of boundary layers

$$\frac{\partial (ru)}{\partial x} + \frac{\partial (rv)}{\partial y} = 0, \tag{8}$$

$$u\frac{\partial u}{\partial x} + v\frac{\partial u}{\partial y} = -\frac{\partial p}{\partial x} + Gr^{1/4}\ \delta_x \frac{\partial p}{\partial y} + \left(1 + \frac{1}{\alpha} \right) \left(1 + \delta_x^2 \right) \frac{\partial^2 u}{\partial y^2} - Mu(E+u) + \theta, \tag{9}$$

$$\delta_x \left(u\frac{\partial u}{\partial x} + v\frac{\partial u}{\partial y} \right) + \delta_{xx} u^2 = -Gr^{1/4}\ \frac{\partial p}{\partial y} + \left(1 + \frac{1}{\alpha} \right) \delta_x \left(1 + \delta_x^2 \right) \frac{\partial^2 u}{\partial y^2} - \theta \tan\gamma, \tag{10}$$

$$u\frac{\partial \theta}{\partial x} + v\frac{\partial \theta}{\partial y} = \frac{1 + \delta_x^2}{Pr} \frac{\partial^2 \theta}{\partial y^2} + Q\theta + M\ Ec\ u(E+u)^2, \tag{11}$$

and the boundary conditions (6) turned out to

$$\begin{aligned} u &= 0, \quad v = 0, \quad \theta = 1 \quad \text{at } y = 0, \\ u &= 0, \quad \theta = 0, \quad p = 0 \quad \text{at } y \longrightarrow \infty. \end{aligned} \tag{12}$$

Here, $M\left(=\frac{\sigma_0 B_0^2 L}{\rho}\right)$, $E\left(=\frac{LE_0}{B_0 \nu Gr^{1/2}}\right)$, $Q\left(=\frac{Q_0 L^2}{\mu C_p Gr^{1/2}}\right)$ $Pr\left(=\frac{\mu C_p}{k}\right)$ and $Ec\left(=\frac{\nu^2 Gr}{C_p\left(\overline{T}_w-\overline{T}_\infty\right)L^2}\right)$ are the magnetic field parameter, electric field parameter, heat generation/absorption parameter, Prandtl number, and Eckert number, respectively.

From Eq. (10), it can be noticed that along y-direction the pressure gradient will be $\mathrm{O}(Gr^{-1/4})$, which means that an inviscid flow solution should be used to evaluate the lowermost order of pressure gradient along x-direction, which leads to $\partial p/\partial x = 0$, for details see [6]. Excluding the terms of the pressure gradient in both Eqs. (9) and (10), thus it is reduced to a single equation

$$u\frac{\partial u}{\partial x}+v\frac{\partial u}{\partial y}+\frac{\delta_x\delta_{xx}}{1+\delta_x^2}u^2=\left(1+\frac{1}{\alpha}\right)\left(1+\delta_x^2\right)\frac{\partial^2 u}{\partial y^2}-\frac{M}{1+\delta_x^2}u(E+u)+\frac{1-\delta_x\tan\gamma}{1+\delta_x^2}\theta. \tag{13}$$

Now, to constringe governing Eqs. (11) and (13) to an opportune form, the following transformations are announced

$$\psi = x^{3/4} r f(x,\eta), \quad \theta=\theta(x,\eta) \quad \text{andalso} \quad \eta = x^{-1/4}y, \quad r = x\sin\gamma, \tag{14}$$

herein ψ is the stream function while η is the pseudo-similarity variable that fulfills Eq. (8) and is realized by

$$u=\frac{1}{r}\frac{\partial \psi}{\partial y}, \qquad v=-\frac{1}{r}\frac{\partial \psi}{\partial x}. \tag{15}$$

On the substitution Eq. (14) in Eqs. (11) and (13), we have

$$\begin{aligned} &x^{1/2}\frac{\partial f}{\partial \eta}\frac{\partial}{\partial x}\left(x^{1/2}\frac{\partial f}{\partial \eta}\right)-\left(\frac{7}{4}f+x\frac{\partial f}{\partial x}\right)\frac{\partial^2 f}{\partial \eta^2}+\frac{\delta_x\delta_{xx}}{1+\delta_x^2}x\left(\frac{\partial f}{\partial \eta}\right)^2 \\ &=\left(1+\frac{1}{\alpha}\right)\left(1+\delta_x^2\right)\frac{\partial^3 f}{\partial \eta^3}-\frac{M}{1+\delta_x^2}x^{1/2}\frac{\partial f}{\partial \eta}\left(E+x^{1/2}\frac{\partial f}{\partial \eta}\right)+\frac{1-\delta_x\tan\gamma}{1+\delta_x^2}\theta, \end{aligned} \tag{16}$$

$$x\left(\frac{\partial f}{\partial \eta}\frac{\partial \theta}{\partial x}-\frac{\partial f}{\partial x}\frac{\partial \theta}{\partial \eta}\right)-\frac{7}{4}f\frac{\partial \theta}{\partial \eta}=\frac{1+\delta_x^2}{Pr}\frac{\partial^2 \theta}{\partial \eta^2}+M\,Ec\,x\frac{\partial f}{\partial \eta}\left(E+x^{1/2}\frac{\partial f}{\partial \eta}\right)^2+Qx^{1/2}\theta. \tag{17}$$

In addition, the boundary conditions in Eq. (12) take the the next formula

$$\begin{aligned} \frac{\partial f}{\partial \eta} &= 0, \quad 7f+4x\frac{\partial f}{\partial \eta}=0, \quad \theta=1 \text{ at } \eta=0, \\ \frac{\partial f}{\partial \eta} &= 0, \quad p=0, \quad \theta=0 \text{ at } \eta\longrightarrow\infty. \end{aligned} \tag{18}$$

The important physical quantities are the local coefficient of skin friction, C_{fx}, and also the local heat transfer rate in form of the local Nusselt number, Nu_x, and they are defined respectively as

$$C_{fx} = \frac{2\tau_w}{\rho U^2}, \qquad Nu_x = \frac{\bar{x} q_w}{k(T_w - T_\infty)}, \tag{19}$$

in which $U = \mu Gr^{1/2}/\rho L$ is characteristic velocity, τ_w and q_w are the shear stress and heat flux at the wall which they are provided respectively by

$$\tau_w = \mu \left(1 + \frac{1}{\alpha}\right) \left(\frac{\partial \overline{u}}{\partial \overline{y}} + \frac{\partial \overline{v}}{\partial \overline{x}}\right)\Bigg|_{\overline{y}=\overline{\sigma}(\overline{x})}, \qquad q_w = -k \sqrt{\left(\frac{\partial \overline{T}}{\partial \overline{x}}\right)^2 + \left(\frac{\partial \overline{T}}{\partial \overline{y}}\right)^2}\Bigg|_{\overline{y}=\overline{\sigma}(\overline{x})}. \tag{20}$$

Applying the non-dimensional quantities (7) and the non-similar transformation (14) on Eq. (20), the local coefficient of skin friction, C_{fx}, and also the local heat transfer rate, Nu_x, can be evidenced by

$$\begin{aligned} C_{fx}\left(\frac{Gr}{x}\right)^{1/4} &= 2\left(1 + \frac{1}{\alpha}\right)\left(1 - \sigma_x^2\right) \frac{\partial^2 f}{\partial \eta^2}(x,0), \\ Nu_x \left(\frac{x}{Gr}\right)^{1/4} &= -x\left(1 + \sigma_x^2\right)^{1/2} \frac{\partial \theta}{\partial \eta}(x,0). \end{aligned} \tag{21}$$

3. NUMERICAL PROCEDURE

Local, not similar, partial differential Eqs. (16) and (17) are integrated along with the boundary conditions (18) by combining the implicit finite difference approximation upon Keller-box method described by Keller [38, 39], Keller and Cebeci [40], Cebeci and Bradshaw [41], and Vajravelu and Prasad [42]. This method is widely used in solving the physical problems, see for example the work of Swalmeh et al. [43] and Ahmad et al. [44].

First, Eqs.(16), (17) and (18) are mutated to a set of a five-order system of equations accordingly these equations are formulated in finite-difference procedures with a second- Newton 's approach is used to linearize nonlinear algebraic equations resulting and has been represented in matrix-vector notation. Resolution of these equations and their boundary conditions through the Thomas algorithm for the block tridiagonal systems. The solution starts at $x = 0$, with the right step size $\Delta\eta$, including interval $0 \leq \eta \leq \eta_\infty$ by iteration, and continues to an iteration of $x > 0$ position with the appropriate step size Δx. The step sizes are $\Delta\eta = 0.02$, and $\Delta x = 0.04$, further, the boundary thickness is $\eta_\infty = 5$. The iterative process was stopped when the error

in computing the wall shear stress parameter $f_{\eta\eta}(x,0)$ in the next procedure convergent criteria 10^{-5}. Furthermore, the technique followed here is unconditionally stable besides realizes extraordinary precision, converges rapidly, and awards stable numerical meshing functionality. MATLAB software (R2018b) provides computations and graphical analyses.

4. RESULTS AND DISCUSSION

In the existence of internal heat generation/ absorption, and Ohmic dissipation, the influence of electric field on forced convection of the electrically incompressible Casson fluid with variable electrical conductivity adjacent to a uniformly heated vertical cone-waved surface were investigated. In an interpretation of the results, numerical calculations for unlike values of the aforementioned five parameters have been carried out using the Keller box method. In the current research problem, we are concentrating our prominence on the influence of magnetic field parameter M, electric field parameter E, Casson fluid parameter α, heat generation/absorption parameter Q, and Eckert number Ec on the velocity, temperature, local skin friction coefficient C_{fx} and local rate of heat transfer Nu_x. It should be mentioned that the value of Prandtl number is fixed at $Pr = 7.2$ for the upcoming figures through this research.

Figs. 2(a) and (b) demonstrate the magnetic parameter M effectiveness on velocity profiles and temperature distributions, respectively. It is observable that M values decrease velocity, while the temperature rises as M increases. It is also seen that at the boundary wall the velocity is zero, where the velocity reaches the highest value as η growths and the velocity finally approaches the asymptotic value. It is well understood that the current passes through the moving fluid by producing a resistive force and therefore this force reduces fluid movement and rises the thermal boundary layer thickness.

Figs. 3(a) and (b) show the behaviors of the velocity profiles and temperature distributions, respectively, for distinctive values of the electric field parameter E. It is noticed from Fig. 3(a) that u dwindles with a growth in E which is consequence of the momentum boundary layer thickness reduces. Truth be told that the Lorentz force grows with increased electrical strength, which makes the fluid flow resistant and thus shrinkages the velocity. Also, from Fig. 3(b), it is depicted that the temperature distributions enhance for expansion for E due to the thickness of thermal boundary heightens by raising of Lorentz force.

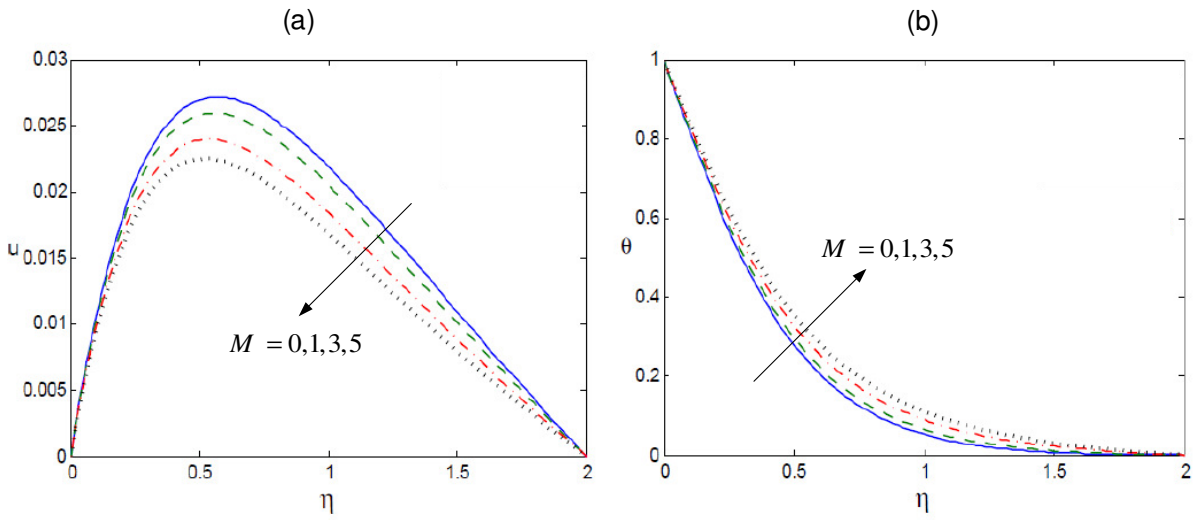

FIGURE 2. The drawing of effectiveness for M on (a) $u(x,\eta)$ and (b) $\theta(x,\eta)$ when $a = 0.2$, $\alpha = 1$, $E = 0.3$, $\gamma = \pi/4$, $Ec = 5$ and $Q = 0.4$.

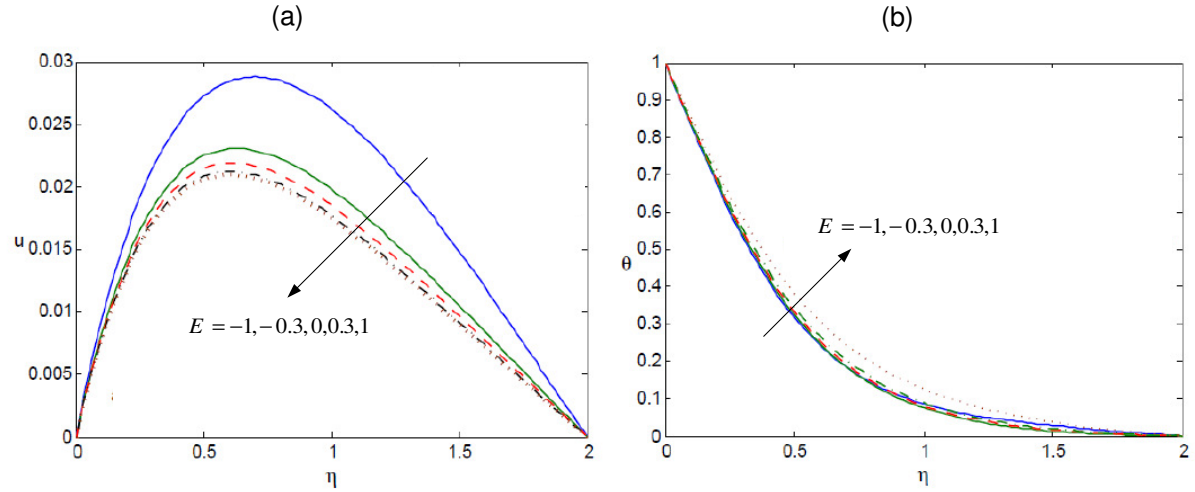

FIGURE 3. The drawing of effectiveness for E on (a) $u(x,\eta)$ and (b) $\theta(x,\eta)$ when $a = 0.2$, $\alpha = 0.5$, $M = 1$, $\gamma = \pi/4$, $Ec = 3$ and $Q = 0.4$.

In the Figs. 4(a) and (b), the impacts on velocity profiles and temperature distributions of the various Casson fluid parameter α values, respectively, are demonstrated. As α rises, the yield stress shrinkages and the thickness of the velocity boundary layer grows accordingly. The velocity is increased in the neighborhood of the wavy surface with an increase in α. This is because a buildup in α yields a reduction in the stress of the Casson fluid. From Fig. 4(b), it is evident that buildups α, the thermal thickness of the boundary layer shrinks and therefore the temperature inside the boundary layer.

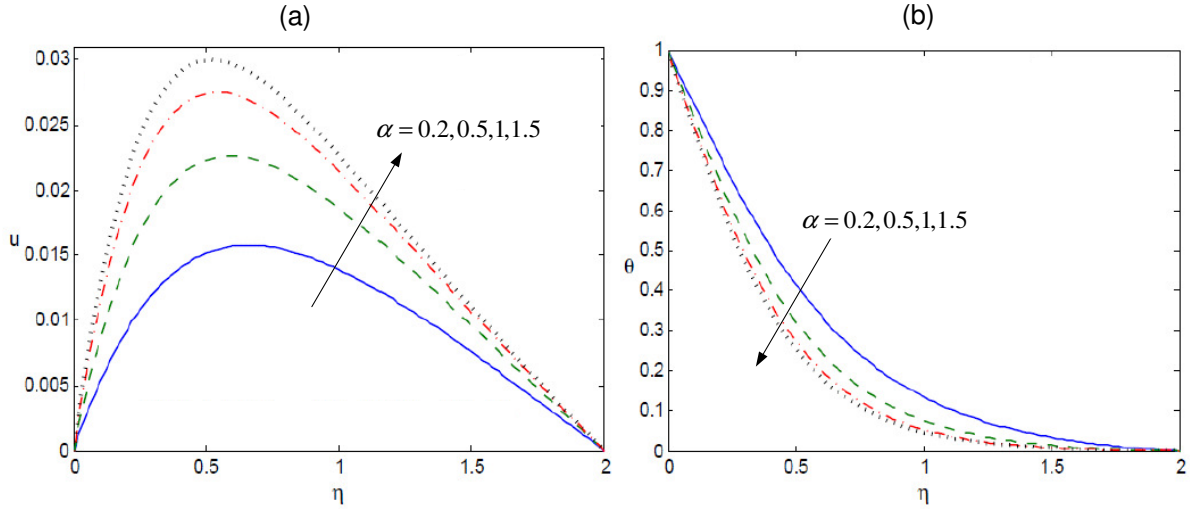

FIGURE 4. The drawing of effectiveness for α on (a) $u(x,\eta)$ and (b) $\theta(x,\eta)$ when $a = 0.1$, $M = 1$, $E = 0.3$, $\gamma = \pi/4$, $Ec = 5$ and $Q = 0.4$.

Figs. 5(a) and (b) explain the change of velocity profiles and temperature distributions on growing the value of heat generation/absorption parameter Q. We can observe from Fig. 5(a) that u decays rapidly to its asymptotic estimates and oncoming to zero in the stream region. Moreover, the velocity achieved to its extreme value away from the wavy surface when Q growths. It is also evident that the thickness of momentum increases and the velocity. Fig. 5(b) reveals that the temperature distribution slightly increase versus the variable values of Q.

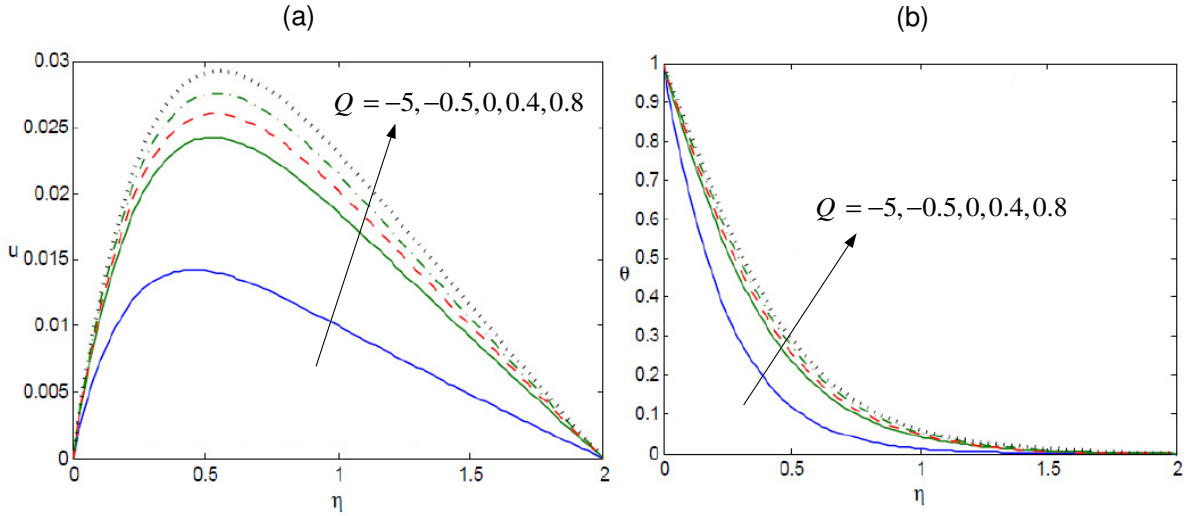

FIGURE 5. The drawing of effectiveness for Q on (a) $u(x,\eta)$ and (b) $\theta(x,\eta)$ when $a = 0.1$, $\alpha = 1$, $M = 1$, $E = 0.3$, $\gamma = \pi/4$ and $Ec = 5$.

Figs. 6(a) and (b) demonstrate the impact of the Eckert number Ec upon the velocity profiles and temperature distributions, respectively. It is noted from Fig. 6(a) that growing value of Ec

rises u. This is because the growing value of Ec elevates thermal energy inside the boundary layer owing to fluid friction which visibly increases convection and eventually increase velocity. The effectiveness of separate Ec on θ is indicated in Fig. 6(b). Likewise contrasted with the instance no viscous dissipation, it comprehends that the temperature may be enhanced for enhancing those Eckert number to every one sorts of fluids. Because of viscous heating, those enhanced in the temperature will be improved and calculable for higher value of Ec. In different words, enhancing those Eckert number prompts a cooling of the surface. Moreover, a transfer of heat into the fluid happens which causes an ascent in the temperature.

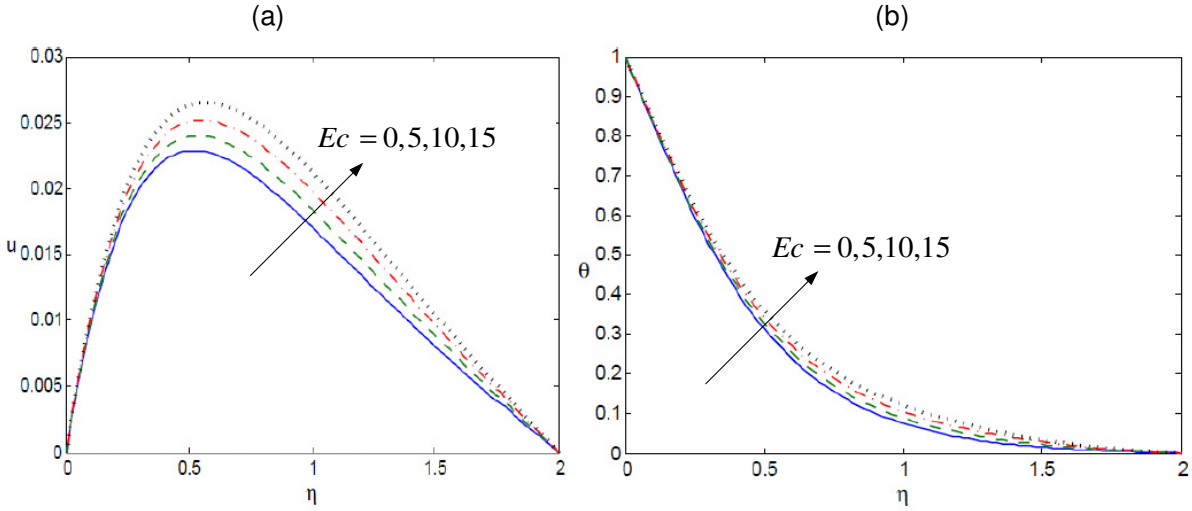

FIGURE 6. The drawing of effectiveness for Ec on (a) $u(x,\eta)$ and (b) $\theta(x,\eta)$ when $a = 0.2$, $\alpha = 1$, $M = 3$, $E = 0.3$, $\gamma = \pi/4$ and $Q = 0.4$.

Figs. 7(a) and (b) exhibit the impact of magnetic field parameter M on local coefficient of skin friction C_{fx} and local heat transfer rate Nu_x, respectively. It is observed that a fall in C_{fx} and local rate of heat transfer due to the reinforcement of M. Similar behavior is noted when the electric field parameter E increases, as shown in Figs. 8(a) and (b).

Figs. 9(a) and (b) present the local coefficient of skin friction C_{fx} and local rate of heat transfer Nu_x for variation in the Casson fluid parameter α. It is detected from Fig. 9(a) that the growth in α produces a decline in C_{fx}. This is forasmuch the enlargement in α causes an intension in the fluid motion. Fig. 9(b) exhibits that the local rate of heat transfer Nu_x rises inasmuch an increase in α. It is because the thickness of thermal boundary layer reduces with α causing the temperature gradient at the cone surface to increase. The influence of the heat

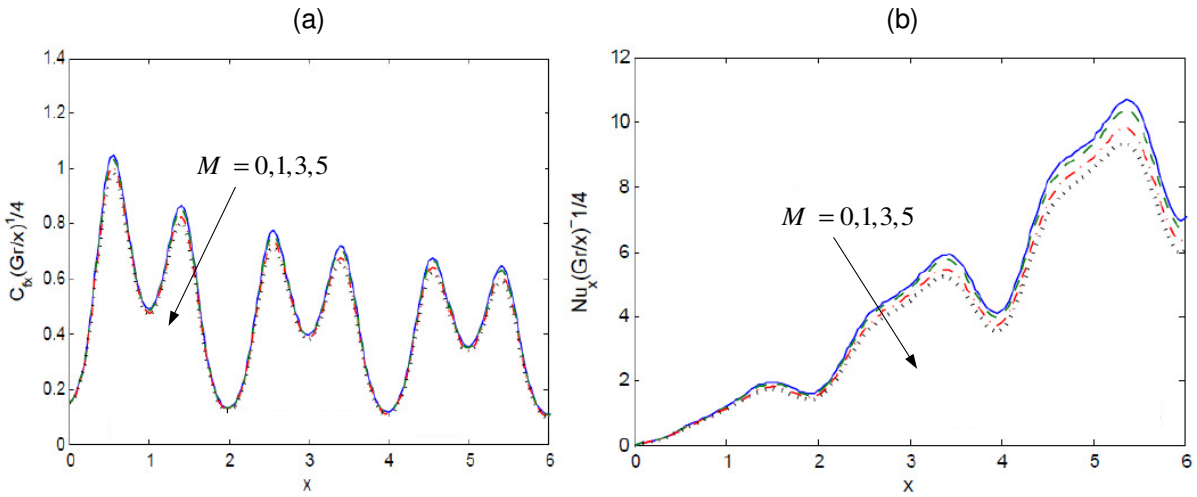

FIGURE 7. The drawing of effectiveness for M on (a) C_{fx} and (b) Nu_x when $a = 0.2$, $\alpha = 1$, $E = 0.3$, $\gamma = \pi/4$, $Ec = 5$ and $Q = 0.4$.

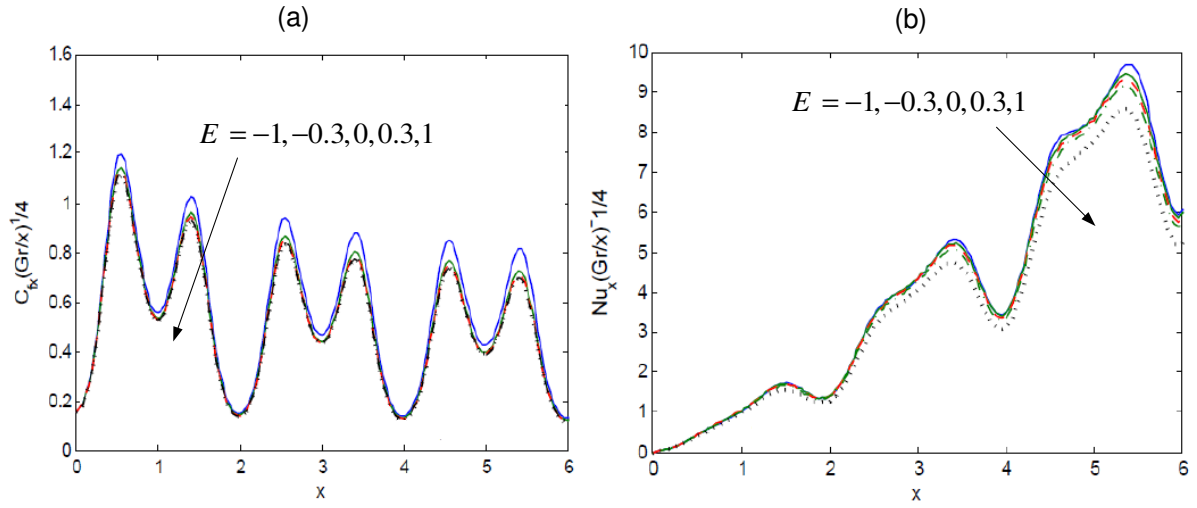

FIGURE 8. The drawing of effectiveness for E on (a) C_{fx} and (b) Nu_x when $a = 0.2$, $\alpha = 0.5$, $M = 1$, $\gamma = \pi/4$, $Ec = 3$ and $Q = 0.4$.

generation/absorption parameter Q on C_{fx} and local heat transfer rate Nu_x is characterized in Figs. 10(a) and (b), respectively. From those, it is depicted that growth in Q leads up to raise the local coefficient of skin friction C_{fx} and reduce Nu_x. These occur due to a change in frictional surface force, and the fluid temperature rise as a result of heat generation/absorption parameter Q values enhance and then surface/fluid temperature difference turn out to be lower and the rate heat transfer rate also reduces.

Figs. 11(a) and (b) elucidate the impact of Eckert number Ec upon local coefficient of skin friction C_{fx} and local heat transfer rate Nu_x. The results of that the excessive value of Ec

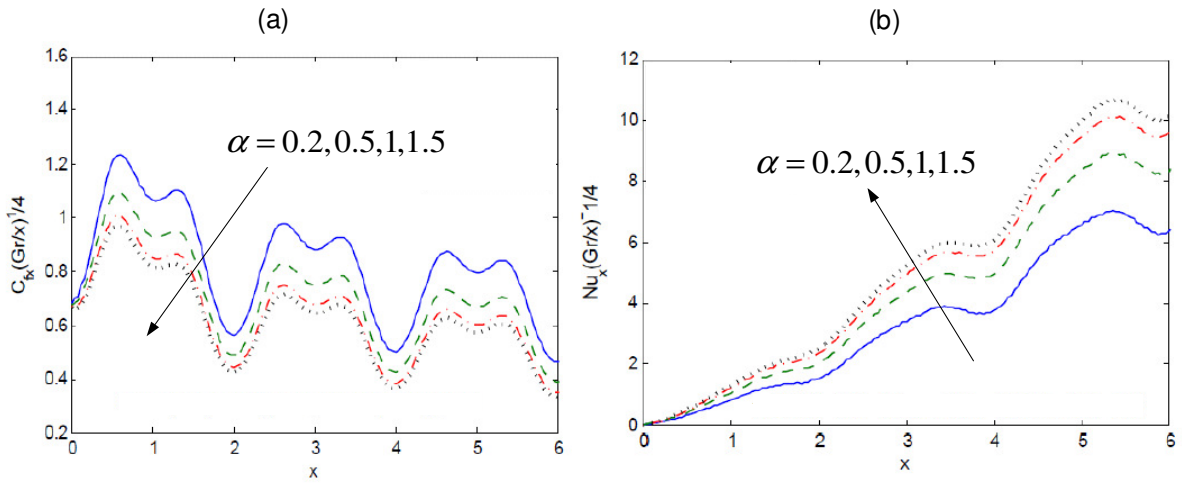

FIGURE 9. The drawing of effectiveness for α on (a) C_{fx} and (b) Nu_x when $a = 0.1$, $M = 1$, $E = 0.3$, $\gamma = \pi/4$, $Ec = 5$ and $Q = 0.4$.

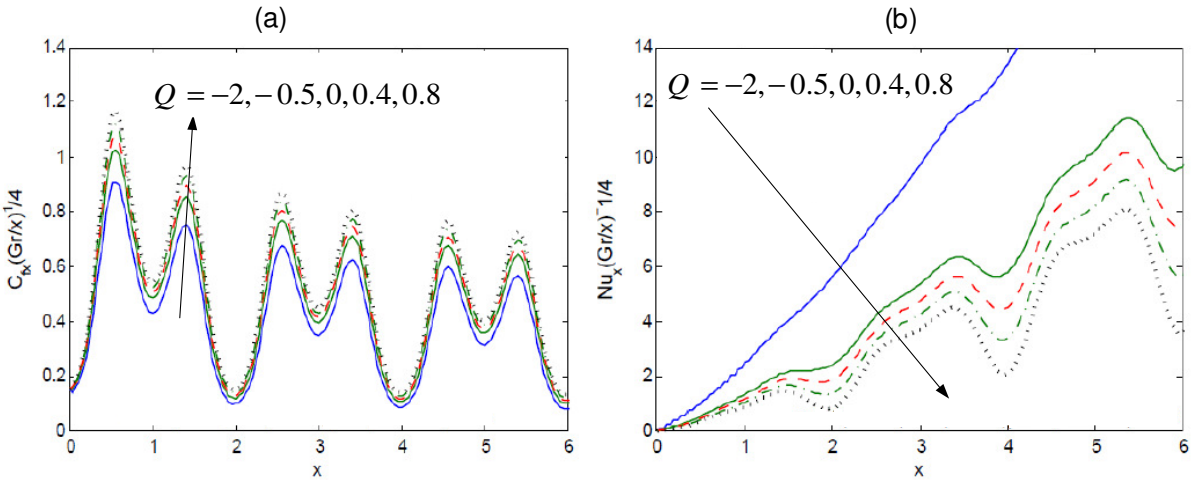

FIGURE 10. The drawing of effectiveness for Q on (a) C_{fx} and (b) Nu_x when $a = 0.2$, $\alpha = 0.5$, $M = 1$, $E = 0.3$, $\gamma = \pi/4$ and $Ec = 3$.

accelerates the fluid flow and enhances the temperature so from those figures it is detected that Ec, C_{fx} enhances on the upstream orientation of the surface to increase Ec and reduces the local heat transfer rate.

5. CONCLUSIONS

In the existent study, concerted influences of electrohydrodynamic and magnetohydrodynamic on Casson fluid and heat transfer characters in a variable electric conductivity with the internal heat generation/absorption besides Ohmic dissipation are scrutinized. The governing

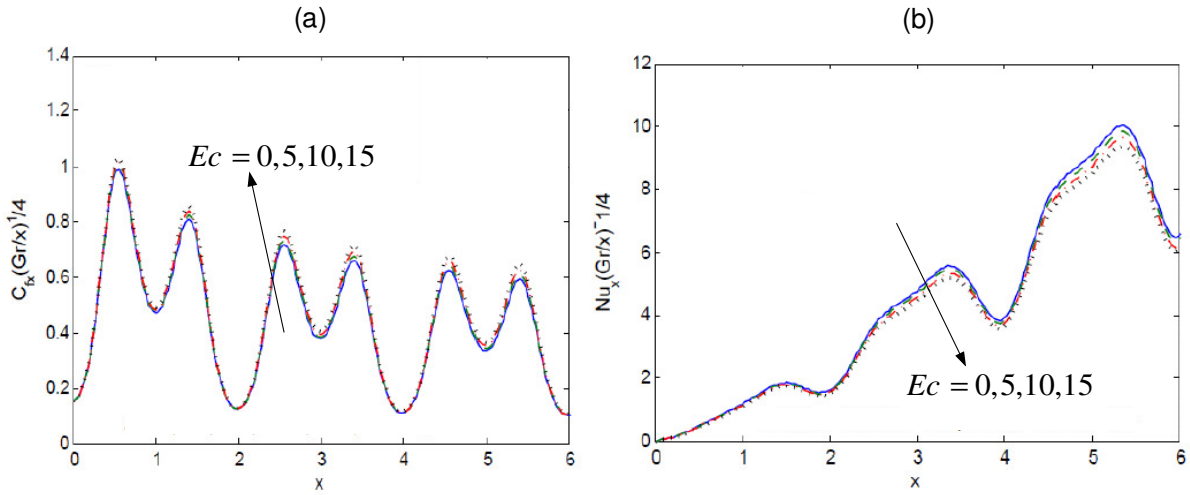

FIGURE 11. The drawing of effectiveness for Ec on (a) C_{fx} and (b) Nu_x when $a = 0.2$, $\alpha = 1$, $M = 3$, $E = 0.3$, $\gamma = \pi/4$ and $Q = 0.4$.

nonlinear partial differential equations to this problem were simplified via the similarity transformations so they could be solved numerically via Keller-box finite difference method. The graphs are structured to analyze the impact of the relevant flow parameters, overall the magnetic field parameter, electric field parameter, Casson fluid parameter, heat generation/absorption parameter, and also Eckert number. The main results have indicated that

- Increasing the electric field parameter and magnetic field parameter, shrink the velocity, local coefficient of skin friction, and local heat transfer rate, further, it elevates the temperature.
- Growing the Casson fluid parameter affords more significantly physically affected, it strongly raises the velocity and local heat transfer rate near the surface but decelerates the temperature and local coefficient of skin friction far away the surface.
- Rising the Eckert number and also the heat generation/absorption parameter enhances the velocity, temperature and local coefficient of skin friction, however, they reduce the local heat transfer rate.
- The velocity is lower when the fluid flows over the rough surface $(a \neq 0)$ compared to the fluid flow over the flat surface $(a = 0)$ while this behavior is reflected with the temperature.

CONFLICT OF INTERESTS

The author(s) declare that there is no conflict of interests.

REFERENCES

[1] I. Pop, Natural convection of a Darcian fluid about a wavy cone, Int. Commun. Heat Mass Transfer 21 (1994), 891-899.

[2] M.A. Hossain, I. Pop, Magnetohydrodynamic boundary layer flow and heat transfer on a continuous moving wavy surface, Arch. Mech. 48 (1996), 813-823.

[3] I. Pop, T.Y. Na, Natural convection over a vertical wavy frustum of a cone, J. Nonlinear Mech. 34 (1999), 925-934.

[4] C.Y. Cheng, Nonsimilar solutions for double diffusive convection near a frustum of a wavy cone in porous media, Appl. Math. Comput. 194 (2007), 156-167.

[5] S. Siddiqa, M. A. Hossain, S. C. Saha, Natural convection ow with surface radiation along a vertical wavy surface, Numer. Heat Transfer, Part A: Appl. 64 (2013), 400-415.

[6] A. Shenoy, M. Sheremet, I. Pop, Convective flow and heat transfer from wavy surfaces: viscous fluids, porous media, and nanofluids, Taylor & Francis, Boca Raton, (2017).

[7] T. Adachi, Y. Takahashi, J. Okajima, Film flow thickness along the outer surface of rotating cones, Eur. J. Mech. B Fluids 68 (2018), 39-44.

[8] S. Siddiqa, N. Begum, A. Quazzi, M.A. Hossain, R.S.R. Gorla, Heat transfer analysis of Casson dusty fluid along a vertical wavy cone with radiating surface, Int. J. Heat Mass Transfer 127 (2018), 589-596.

[9] H. Hanif, I. Khan, S. Shafie, MHD natural convection in cadmium telluride nanofluid over a vertical cone embedded in a porous medium, Phys. Scr. 94 (2019), 125208.

[10] A. Chattopadhyay, S.K. Pandit, H.F. Oztop, An analysis of thermal performance and entropy generation in a wavy enclosure with moving walls, Eur. J. Mech. B Fluids 79 (2020), 12-26.

[11] Boa-Teh Chu, Thermodynamics of electrically conducting fluids, Phys. Fluids 2 (1959), 473-484.

[12] P.H.G. Allen, T.G. Karayiannis, Electrohydrodynamic enhancement of heat transfer and fluid flow, Heat Recov. Syst. CHP. 15 (1995), 389–423.

[13] F.M. Hady, R.A. Mohamed, A. Mahdy, MHD free convection flow along a vertical wavy surface with heat generation or absorption effect, Int. Commun. Heat Mass Transfer 33 (2006), 1253-1263.

[14] M.F. El-Sayed, M.I. Syam, Electrohydrodynamic instability of a dielectric compressible liquid sheet streaming into an ambient stationary compressible gas, Arch. Appl. Mech. 77 (2007), 613–626.

[15] M.F. El-Sayed, Onset of electroconvective instability of Oldroydian viscoelastic liquid layer in Brinkman porous medium, Arch. Appl. Mech. 78 (2008), 211–224.

[16] M.F. El-Sayed, Instability of two streaming conducting and dielectric bounded fluids in porous medium under time-varying electric field, Arch. Appl. Mech. 79 (2009), 19–39.

[17] H.B. Rokni, D.M. Alsaad, P. Valipour, Electrohydrodynamic nanofluid flow and heat transfer between two plates, J. Mol. Liq. 216 (2016), 583-589.

[18] A.K. Pandey, M. Kumar, MHD flow inside a stretching/shrinking convergent/divergent channel with heat generation/absorption and viscous-ohmic dissipation utilzing Cu-water nanofluid, Comput. Therm. Sci. 10 (2018), 457-471.

[19] Kh. Hameed, H. Muhammad, S. Zahir, I. Saeed, Kh. Waris, M. Sher, The combined magneto hydrodynamic and electric field effect on an unsteady Maxwell nanofluid flow over a stretching surface under the influence of variable heat and thermal radiation, Appl. Sci. 8 (2018), 160-177.

[20] H. Thameem Basha, I.L. Animasaun, O.D. Makinde, R. Sivaraj, Effect of Electromagnetohydrodynamic on Chemically Reacting Nanofluid Flow over a Cone and Plate, in: B. Rushi Kumar, R. Sivaraj, B.S.R.V. Prasad, M. Nalliah, A.S. Reddy (Eds.), Applied Mathematics and Scientific Computing, Springer International Publishing, Cham, 2019: pp. 99–107.

[21] A. Mishra, A.K. Pandey, M. Kumar, Numerical investigation of heat transfer of MHD nanofluid over a vertical cone due to viscous-ohmic dissipation and slip boundary conditions, Nanosci. Technol. 10 (2019), 169-193.

[22] N. Kasayapanand, T. Kiatsiriroat, EHD enhanced heat transfer in wavy channel, Int. Commun. Heat Mass Transfer 32 (2005), 809-821.

[23] K.H. Kabir, Md. A. Alim, L.S. Andallah, Effects of viscous dissipation on MHD natural convection flow along a vertical wavy surface, J. Theor. Appl. Phys. 7 (2013), 31-39.

[24] R. Sivaraj, B.R. Kumar, Viscoelastic fluid flow over a moving vertical cone and flat plate with variable electric conductivity, Int. J. Heat Mass Transfer 61 (2013), 119-128.

[25] M. Sheikholeslami, T. Hayat, A. Alsaedi, S. Abelman, Numerical analysis of EHD nanofluid force convective heat transfer considering electric field dependent viscosity, Int. J. Heat Mass Transfer 108 (2017), 2558-2565.

[26] J.Y. Jang, C.C. Chen, 3-D EHD enhanced natural convection over a horizontal plate flow with optimal design of a needle electrode system, Energies 11 (2018), 1670.

[27] S.U. Khan, H. Waqas, S. A. Shehzad, M. Imran, Theoretical analysis of tangent hyperbolic nanoparticles with combined electrical MHD, activation energy and Wu's slip features: a mathematical model, Phys. Scr. 94 (2019), 125211.

[28] H.R. Kataria, H.R. Patel, Effects of chemical reaction and heat generation/absorption on magnetohydrodynamic (MHD) Casson fluid flow over an exponentially accelerated vertical plate embedded in porous medium with ramped wall temperature and ramped surface concentration, Propul. Power Res. 8 (2019), 35-46.

[29] W.A. Khan, A.M. Rashad, M.M.M. Abdou, I. Tlili, Natural bioconvection flow of a nanofluid containing gyrotactic microorganisms about a truncated cone, Eur. J. Mech. B Fluids 75 (2019) 133-142.

[30] N.A. Casson, A flow equation for pigment-oil suspensions of the printing ink type. In C.C. Mill (Ed.), Rheology of disperse suspensions, Pergamon Press, New York (1959).

[31] N.T.M. Eldabe, M.F. El-Sayed, A.Y. Ghaly, H.M. Sayed, Mixed convective heat and mass transfer in a non-Newtonian fluid at a peristaltic surface with temperature-dependent viscosity, Arch. Appl. Mech. 78 (2008), 599–624.

[32] Z. Iqbal, R. Mehmood, E. Azhar, Mehmood, Impact of inclined magnetic field on micropolar Casson fluid using Keller box algorithm, Eur. Phys. J. Plus 132 (2017), 1-13.

[33] A. Mahdy, S.E. Ahmed, Unstreay natural convection heat and mass transfer of non-Newtonian Casson fluid along a vertical wavy surface, Int. J. Mech. Mech. Eng. 11 (2017), 1284-1291.

[34] S. Siddiqa, N. Begum, A. Quazzi, Md.A. Hossain, R.S.R. Gorla, Heat transfer analysis of Casson dusty fluid flow along a vertical wavy cone with radiating surface, Int. J. Heat Mass Transfer 127 (2018), 589-596.

[35] Z. Shah, A. Dawar, I. Khan, S. Islam, D.L.C. Ching, A.Z. Khan, Cattaneo-Christov model for electrical magnetite micropoler Casson ferrofluid over a stretching/shrinking sheet using effective thermal conductivity model, Case Stud. Therm. Eng. 13 (2019), 100352.

[36] F.A. Alwawi, H.T. Alkasasbeh, A.M. Rashad, R. Idris, MHD natural convection of Sodium Alginate Casson nanofluid over a solid sphere, Res. Phy. 16 (2020), 102818.

[37] ATM. M. Rahman, M.S. Alam, M.A. Alim, M.K. Chowdhury, Unsteady MHD forced convective heat and mass transfer flow along a wedge with variable electric conductivity and thermophoresis, Proc. Eng. 56 (2013), 531-537.

[38] H.B. Keller, Numerical methods in bounday layer theory, Annu. Rev. Fluid Mech. 10 (1978), 417-433.

[39] H.B. Keller, A new difference scheme for parabolic problems. In Numerical Solution of Partial Differential Equations – II, Synspade (1970) 327-350. Academic Press, Inc. (1971).

[40] H.B. Keller, T. Cebeci, Accurate numerical methods for boundary-layer flows. II Two-dimensional turbulent flows, AIAA J. 10 (1972), 1193-1199.

[41] T. Cebeci, P. Bradshaw, Physical and computational aspects of convective heat transfer, Springer, Berlin (1984).

[42] K. Vajravelu, K.V. Prasad, Keller-box method and its Application, De Gruyter/Higher Education Press, Berlin (2014).

[43] M.Z. Swalmeh, H.T. Alkasasbeh, A. Hussanan, M. Mamat, Heat transfer flow of Cu-water and Al_2O_3-water micropolar nanofluids about a solid sphere in the presence of natural convection using Keller-box method, Results Phys. 9 (2018), 717-724.

[44] I. Ahmad, M. Faisal, T. Javed, Bi-directional stretched nanofluid flow with Cattaneo-Christov double diffusion, Results Phys. 16 (2019), 102518.